Control of antioxidative response by the tumor suppressor protein PML through regulating Nrf2 activity

Shuang Guo[a], Xiwen Cheng[a], Jun-Hee Lim[a], Yu Liu[a], and Hung-Ying Kao[a,b]
[a]Department of Biochemistry, Case Western Reserve University, Cleveland, OH 44106; [b]Comprehensive Cancer Center of Case Western Reserve University and University Hospitals of Cleveland, Cleveland, OH 44106

ABSTRACT **Oxidative stress is a consequence of an imbalance between reactive oxygen species (ROS) production and the ability of the cytoprotective system to detoxify the reactive intermediates. The tumor suppressor promyelocytic leukemia protein (PML) functions as a stress sensor. Loss of PML results in impaired mitochondrial complex II activity, increased ROS, and subsequent activation of nuclear factor erythroid 2–related factor 2 (Nrf2) antioxidative pathway. We also demonstrate that sulforaphane (SFN), an antioxidant, regulates Nrf2 activity by controlling abundance and subcellular distribution of PML and that PML is essential for SFN-mediated ROS increase, Nrf2 activation, antiproliferation, antimigration, and antiangiogenesis. Taking the results together, we have uncovered a novel antioxidative mechanism by which PML regulates cellular oxidant homeostasis by controlling complex II integrity and Nrf2 activity and identified PML as an indispensable mediator of SFN activity.**

Monitoring Editor
A. Gregory Matera
University of North Carolina

Received: Nov 20, 2013
Revised: May 1, 2014
Accepted: Jun 10, 2014

INTRODUCTION

Oxidative stress is a consequence of an imbalance between reactive oxygen species (ROS) production and the ability of the cytoprotective system to detoxify the reactive intermediates. Basal levels of reactive intermediates are critical for relaying signal transduction and the maintenance of cellular function (Sena and Chandel, 2012). However, excessive production of ROS leads to oxidative stress and is correlated with the onset and progression of many diseases, such as atherosclerosis, diabetes, neurodegeneration, and cancer (Andersen, 2004; Nishikawa and Araki, 2007; Heistad *et al.*, 2009; Trachootham *et al.*, 2009). Nuclear factor erythroid 2–related factor 2 (Nrf2) is a member of the cap'n'collar-related basic region-leucine zipper transcription factors and plays a pivotal role in the cellular defense system against oxidative stress (Moi *et al.*, 1994; Itoh *et al.*, 1997). In resting cells, Nrf2 resides in the cytosol through association with Kelch-like ECH-associated protein 1 (Keap1). Keap1 complexes with cullin 3 to form a ubiquitin E3 ligase that acts as a substrate adaptor that binds Nrf2 and promotes its ubiquitination-dependent proteasomal degradation (Itoh *et al.*, 1999). Upon ROS exposure, several reactive cysteine residues in Keap1 are covalently modified, resulting in Keap1 inactivation and subsequent stabilization and nuclear translocation of Nrf2 (Zhang and Hannink, 2003). Nuclear Nrf2 heterodimerizes with a small Maf protein and binds to antioxidant response elements (AREs) in the promoter regions of a subset of antioxidative genes that includes NAD(P)H dehydrogenase [quinone] 1 (*NQO1*; Venugopal and Jaiswal, 1996; Tong *et al.*, 2006; Yamamoto *et al.*, 2008). Induction of Nrf2 by ROS leads to a marked increase in the expression of target genes that protect the cells from oxidative stress–mediated cytotoxicity (Itoh *et al.*, 1997). In addition to antioxidative enzymes, Nrf2 target genes also include cytoprotective genes involved in several protective systems, such as conjugating/detoxification enzymes, molecular chaperones, transporters, and anti-inflammatory signaling molecules (Kensler *et al.*, 2007).

Sulforaphane (SFN) belongs to the isothiocyanate family and is widely used as an antioxidant supplement and applied in cancer chemoprevention. The precursor of SFN, glucoraphanin, is abundant in cruciferous vegetables, with the highest concentration found in broccoli (Zhang *et al.*, 1992). Among known SFN targets, Keap1,

This article was published online ahead of print in MBoC in Press (http://www.molbiolcell.org/cgi/doi/10.1091/mbc.E13-11-0692) on June 18, 2014.

Address correspondence to: Hung-Ying Kao (hxk43@cwru.edu)

Abbreviations used: APL, acute promyelocytic leukemia; ARE, antioxidant response element; ChIP, chromatin immunoprecipitation; CHX, cycloheximide; DAPI, 4′,6-diamidino-2-phenylindole; EC, endothelial cell; HUVEC, human umbilical vein endothelial cell; Keap1, Kelch-like ECH-associated protein 1; MEF, mouse embryonic fibroblast; NAC, *N*-acetyl cysteine; NB, nuclear body; NQO1, NAD(P)H dehydrogenase [quinone] 1; Nrf2, nuclear factor erythroid 2–related factor 2; PML, promyelocytic leukemia protein; ROS, reactive oxygen species; SFN, sulforaphane.

which serves as an adaptor protein for a cullin 3–dependent E3 ubiquitin ligase complex–mediated degradation of substrates such as Nrf2, is most extensively studied (Zhang *et al.*, 2004). SFN reacts with the thiol groups on several cysteine residues of Keap1, thereby disrupting its association with cullin 3 and relieving its inhibitory activity on its target proteins such as Nrf2. Inactivation of Keap1 leads to nuclear translocation of Nrf2 and subsequent induction of its target genes (Thimmulappa *et al.*, 2002; Hong *et al.*, 2005). Of note, many reports have suggested that SFN can impinge on apoptotic signaling pathways in cancer cells with various origins (Gamet-Payrastre *et al.*, 2000; Fimognari *et al.*, 2002; Pham *et al.*, 2004; Singh *et al.*, 2004; Mi *et al.*, 2007; Pledgie-Tracy *et al.*, 2007) and possesses antiproliferative and antiangiogenic activity in endothelial cells (ECs; Asakage *et al.*, 2006; Nishikawa *et al.*, 2010).

The promyelocytic leukemia protein (PML) was originally identified as a fusion partner with human retinoic acid receptor α due to a chromosomal translocation found in patients with acute promyelocytic leukemia (APL; Melnick and Licht, 1999). PML-knockout mice are viable, but loss of PML renders the mice sensitive to spontaneous and chemically induced tumorigenesis (Wang *et al.*, 1998). In contrast, overexpression of PML often results in senescence, cell cycle arrest, and apoptosis (Mu *et al.*, 1997). PML is primarily found in discrete nuclear structures referred to as PML nuclear bodies (NBs; Stuurman *et al.*, 1992). PML NBs are dynamic structures that are the targets of various extracellular stimuli (Reineke and Kao, 2009; Lallemand-Breitenbach and de The, 2010). In most cell types, the number and size of PML NBs increase in response to cellular stresses, which has led to the belief that PML NBs are stress-responsive structures (Maul *et al.*, 1995; Eskiw *et al.*, 2003; Seker *et al.*, 2003; Salomoni *et al.*, 2005).

However, whereas the role of PML and its regulation have been intensively studied in cancer cells, its role in ECs remains largely unknown. Our lab recently showed that PML is required for tumor necrosis factor α– and interferon α–mediated inhibition of EC migration and in vitro network formation (Cheng *et al.*, 2012). In the vasculature, ROS can be generated in ECs. ROS levels are linked to protein aggregation and misfolding when cells are maintained in culture for prolonged periods (Farout and Friguet, 2006). ROS-dependent aggregation of proteins including PML has been identified in certain cell lines (Moran *et al.*, 2009). Recent studies indicate that PML is an oxidative stress sensor and its abundance is regulated by oxidative stress inducers. For example, PML is subjected to ubiquitin- and small ubiquitin-like modifier–dependent degradation by As_2O_3 treatment, which serves as a mechanism for the therapeutic effects of As_2O_3 in APL patients (de The *et al.*, 2012; Lallemand-Breitenbach *et al.*, 2012). Direct binding of As_2O_3 to specific cysteines of PML has also been reported and is suggested to play a significant role in As_2O_3-mediated PML degradation (Jeanne *et al.*, 2010; Zhang *et al.*, 2010). High doses of H_2O_2 stabilize PML protein, which in turn mediates H_2O_2-induced apoptosis in breast cancer cells (Reineke *et al.*, 2008). High doses of H_2O_2 also induce nuclear accumulation and deacetylation of PML in HeLa cells (Guan, Lim, Peng, Liu, Lam, Seto, and Kao, unpublished results). In contrast, PML protein accumulation is down-regulated in cells treated with low concentrations of H_2O_2 in human umbilical vein endothelial cells (HUVECs; Han *et al.*, 2010). In this study, we report that PML plays a crucial role in regulating abundance, nuclear accumulation, and *trans*-activating capacity of Nrf2 by regulating ROS accumulation. We also identify PML as an integral component of SFN-induced Nrf2 activation, antiproliferation, antimigration, and antiangiogenic activities.

RESULTS

Loss of PML increases Nrf2 protein abundance and stability

Using a small interfering RNA (siRNA) knockdown approach and microarray gene expression analysis, we found that the expression of a cluster of genes related to antioxidative pathways was altered in PML-knockdown HUVECs. Many of the antioxidant genes up-regulated in PML-knockdown cells were known downstream targets of Nrf2 (Figure 1A). This observation was further confirmed by immunoblotting of HUVEC extracts, which showed that the protein abundance of Nrf2 and NQO1 were elevated in PML-knockdown cells (Figure 1B). We detected multiple bands of Nrf2, which appear to be distinct isoforms, because the intensity of all the bands detected between 65 and 120 kDa was significantly decreased by two independent Nrf2 siRNAs (Supplemental Figure S1A). We also suggest that the slowest-migrating species of Nrf2 is a phosphorylated form, since it disappears in phosphatase-treated samples (Supplemental Figure S1B). Furthermore, cell-based sumoylation assays indicated that the slower-migrating Nrf2 species was not sumoylated Nrf2 (Supplemental Figure S1, C and D). Consistent with our observations in HUVECs, increased protein levels of Nrf2 and its target NQO1 were also observed in $Pml^{-/-}$ mouse embryonic fibroblasts (MEFs) compared with those in $Pml^{+/+}$ MEFs (Figure 1C). Because of the essential role of liver in antioxidative defense and detoxification, we examined liver isolated from $Pml^{+/+}$ and $Pml^{-/-}$ mice and found that $Pml^{-/-}$ liver expressed slightly higher levels of Nrf2 and NQO1 than those in the $Pml^{+/+}$ liver (Figure 1D). In contrast, Nrf2 and NQO1 were down-regulated in HeLa cells when PML isoforms 1 and 4 were ectopically overexpressed (Figure 1E), and additive effects on Nrf2 were observed when PML1 and PML4 were coexpressed (Figure 1F). Similarly, exogenously expressed Nrf2 was down-regulated after PML overexpression (Figure 1G), suggesting that the stability of Nrf2 might be affected by PML abundance. To test this, we cotransfected an Nrf2 expression plasmid with or without a PML4 expression plasmid and treated the cells with cycloheximide (CHX), an inhibitor of protein synthesis. We found that the half-life of Nrf2 was decreased in PML-overexpressing cells compared with the control (no PML overexpression; Figure 1H). Collectively our evidence points to a role for PML as a negative regulator of Nrf2 activity by reducing its protein accumulation and stability.

PML inhibits nuclear accumulation and *trans*-activating capacity of Nrf2

Because the stability of Nrf2 is directly linked to its nuclear accumulation, we performed subcellular fractionation in $Pml^{+/+}$ and $Pml^{-/-}$ MEFs and found that the nuclear fraction contained significantly more Nrf2 in $Pml^{-/-}$ MEFs than in $Pml^{+/+}$ MEFs, whereas the amount in the cytoplasmic fraction was only slightly altered (Figure 2A). Of interest, the slower-migrating Nrf2 species were predominantly found in the nucleus. Immunofluorescence microscopy also indicated that Nrf2 accumulated to a greater extent in nuclei of $Pml^{-/-}$ MEFs than in $Pml^{+/+}$ MEFs (Figure 2B). In contrast, nuclear Nrf2 was minimally detectable when PML was overexpressed in HeLa cells compared with control cells, whereas cytoplasmic Nrf2 was also decreased by PML overexpression, as indicated by immunoblotting and immunofluorescence microscopy (Figure 2, C and D). A similar observation was obtained in HUVECs (Figure 2E). We conclude that the nuclear accumulation of Nrf2 is significantly up-regulated in $Pml^{-/-}$ MEFs and reduced in cells overexpressing PML.

To further dissect whether nuclear or cytoplasmic PML affects Nrf2 protein abundance, we used a PML mutant, K487R, which is constitutively localized in the cytoplasm (Supplemental Figure S2). Overexpression of PML (K487R) had no effect on Nrf2 protein

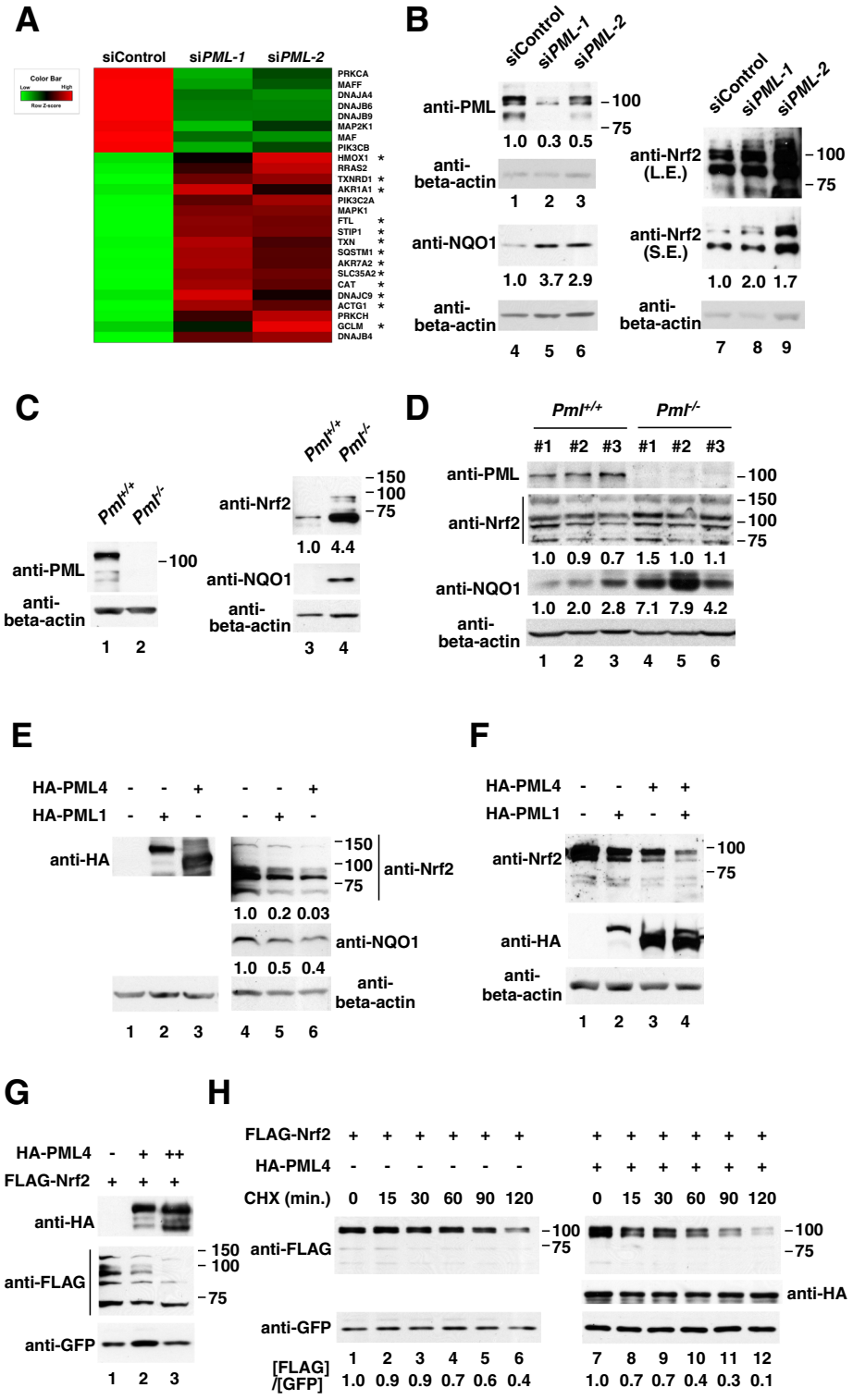

FIGURE 1: PML negatively regulates Nrf2 protein abundance and its downstream target genes. (A) A heat map of significantly altered genes (greater than twofold, $p < 0.01$) involved in antioxidant pathways identified by microarray gene expression analysis in PML-knockdown HUVECs. siControl represents control siRNA, and si*PML*-1 and si*PML*-2 represent two independent PML siRNAs targeting different regions of PML mRNA. Asterisks mark known Nrf2 target genes. (B) The effects of PML knockdown on Nrf2 and NQO1 protein abundance in HUVECs. HUVECs were transfected with a nontargeting siRNA or two independent PML siRNAs for 72 h. Cell extracts were analyzed by immunoblotting with the indicated antibodies. β-Actin was used as a loading control. Relative intensities of the bands are normalized to both loading control and siControl. L.E., longer exposure; SE, shorter exposure. (C) Nrf2 and NQO1 protein expression in $Pml^{+/+}$ and $Pml^{-/-}$ MEFs. Relative intensities of the bands are normalized to both loading control and $Pml^{+/+}$. (D) Nrf2 and NQO1 protein expression in $Pml^{+/+}$ and $Pml^{-/-}$ liver. Liver homogenates were prepared from 3 $Pml^{+/+}$ and 3 $Pml^{-/-}$ mice. Relative intensities of the bands are normalized to both loading control and $Pml^{+/+}$ #1. (E) The effects of PML1 or PML4 overexpression on endogenous Nrf2 protein abundance in HeLa cells. HeLa cells were transfected with plasmids expressing HA-tagged PML1 or PML4. Relative intensities of the bands are normalized to both loading control and vector control. (F) The effects of PML1 and PML4 coexpression on endogenous Nrf2 protein abundance in HeLa cells. HeLa cells were transfected with plasmids expressing HA-tagged PML1, PML4, or PML1 combined with PML4. (G) The effects of PML1 or PML4 overexpression on cotransfected Nrf2 protein abundance in HeLa cells. HeLa cells were transfected with plasmids expressing FLAG-tagged Nrf2, GFP, and different amounts of HA-tagged PML4. GFP was cotransfected and used as a transfection and loading control. (H) The effects of PML4 overexpression on the half-life of cotransfected Nrf2 in HeLa cells. HeLa cells were transfected with plasmids expressing FLAG-tagged Nrf2 and GFP with or without HA-tagged PML4. After 24 h, cells were replated for CHX treatments. CHX was added to the medium at 20 μg/ml for 0, 15, 30, 60, 90, and 120 min. Relative intensities of the bands are normalized to both loading control and 0 min.

abundance, whereas restoring localization of this mutant to the nucleus by adding a nuclear localization sequence (NLS) resulted in similar effects as wild type (Figure 2F and Supplemental Figure S2). Exogenous overexpressed Nrf2 was also subjected to reduction by the nuclear mutant of PML (Supplemental Figure S3). These data suggest that decreases in nuclear Nrf2 accumulation were primarily mediated by nuclear forms of PML.

Because nuclear Nrf2 activates its target genes through binding to ARE-containing promoter regions, we next examined Nrf2 target gene expression. As expected, a battery of Nrf2 target genes that contain AREs in their promoter regions were up-regulated in $Pml^{-/-}$ MEFs (Figure 3A) and liver tissue isolated from $Pml^{-/-}$ mice (Figure 3B). We further tested the promoter activity of an ARE-containing luciferase reporter under conditions of PML overexpression and found that the promoter activity was significantly down-regulated by PML in a dose-dependent manner (Figure 3C). Using chromatin immunoprecipitation (ChIP) assays, we observed that there was less binding of Nrf2 on the AREs of the *NQO1* (Figure 3D) and *HO-1* promoters (Figure 3E) in PML-overexpressing

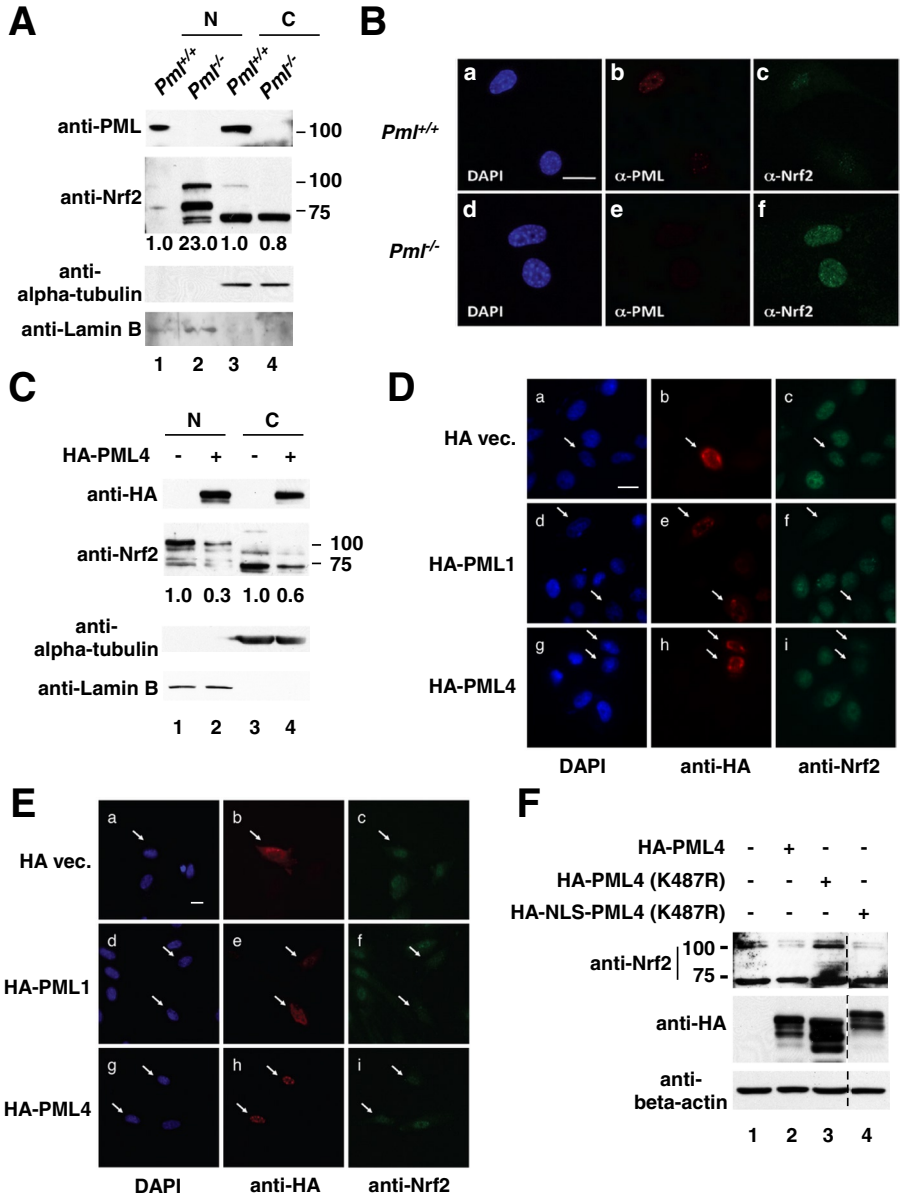

FIGURE 2: PML inhibits nuclear accumulation of Nrf2. (A) Subcellular fractionation and immunoblotting analysis of $Pml^{+/+}$ and $Pml^{-/-}$ MEFs. Nuclear and cytoplasmic fractions prepared from $Pml^{+/+}$ and $Pml^{-/-}$ MEFs were subjected to immunoblotting analysis with the indicated antibodies. Lamin B and α-tubulin were used as loading controls for nuclear and cytoplasmic fractions, respectively. Relative intensities of the bands are normalized to both loading control and $Pml^{+/+}$. N, nucleus; C, cytoplasm. (B) Immunofluorescence analysis of MEFs. Cells were immunostained with anti-PML and anti-Nrf2 antibodies, and images were taken by a fluorescence microscope. DAPI-stained nuclei (a, d); PML (b, e); Nrf2 (c, f). Scale bar, 20 μm. (C) Subcellular fractionation and immunoblotting analysis of HeLa cells with PML overexpression. HeLa cells were transfected with plasmids expressing HA-tagged PML4. Nuclear and cytoplasmic fractions prepared from transfected HeLa cells were subjected to immunoblotting analysis with the indicated antibodies. Relative intensities of the bands are normalized to both loading control and vector control. N, nucleus; C, cytoplasm. (D) Immunofluorescence analysis of HeLa cells with PML1 or PML4 overexpression. HeLa cells were transfected with plasmids expressing HA-tagged PML1 or PML4. Cells were immunostained with anti-HA and anti-Nrf2 antibodies, and images were taken on a fluorescence microscope. DAPI-stained nuclei (a, d, g); HA-tagged PML (b, e, h); endogenous Nrf2 (c, f, i). The arrows mark cells expressing transfected PML. Scale bar, 20 μm. (E) Immunofluorescence analysis of HUVECs with PML1 or PML4 overexpression. The experiments were performed as described in D. (F) The effects of nuclear and cytoplasmic mutants of PML4 overexpression on endogenous Nrf2 protein abundance in HeLa cells. HeLa cells were transfected with plasmids expressing HA-tagged PML4 (wild type), PML4 (K487R), and NLS-PML4 (K487R). Dividing line marks edges of different parts of the same gel.

HeLa cells. Furthermore, recruitment of Nrf2 to the *NQO1*-ARE was increased in PML-knockdown HUVECs (Figure 3F). These results lead to the conclusion that loss of PML leads to accumulation of nuclear Nrf2 and elevation in the *trans*-activating capacity of Nrf2 on ARE-driven gene expression.

ROS play a role in PML-mediated Nrf2 regulation

Previous studies demonstrated that nuclear Nrf2 is induced in response to increases in ROS accumulation (Zhang and Hannink, 2003; Yamamoto *et al.*, 2008). We hypothesized that loss of PML may impair redox homeostasis, leading to an accumulation of excess ROS. To test this, we measured ROS levels in $Pml^{+/+}$ and $Pml^{-/-}$ MEFs via a fluorescence-based assay and observed a twofold increment of ROS accumulation in $Pml^{-/-}$ MEFs compared with those in $Pml^{+/+}$ MEFs (Figure 4A). Similarly, ROS levels were up-regulated in PML-knockdown HUVECs (Figure 4B). Conversely, ROS production was reduced by PML overexpression in a dose-dependent manner (Figure 4C). Furthermore, only wild-type or nuclear PML (HA-NLS-PML4 [K487R]) was capable of reducing ROS accumulation (Figure 4D). Because the major source of endogenous ROS is mitochondrial respiration (Raha and Robinson, 2000), we asked whether mitochondrial respiration was defective in $Pml^{-/-}$ mice. Mitochondrial complexes I–III contribute to ROS accumulation (Paddenberg *et al.*, 2003; Calkins *et al.*, 2005; Ishii *et al.*, 2005; Guzy *et al.*, 2008). Using liver tissue derived from $Pml^{+/+}$ and $Pml^{-/-}$ mice, we performed complex I and complex II enzyme activity assays. We observed little or no difference in complex I activity between $Pml^{+/+}$ and $Pml^{-/-}$ liver tissue (Cheng *et al.*, 2013) but a dramatic reduction of complex II enzymatic activity in liver derived from $Pml^{-/-}$ mice (Figure 4E). In addition, we detected a global reduction of genes encoding subunits of complex II (*Sdha-d*) or factors (*Sdhaf1* and *Sdhaf2*) required for complex II assembly in liver from $Pml^{-/-}$ mice (Figure 4F), suggesting that complex II dysfunction observed in $Pml^{-/-}$ mice is, in part, due to reduced complex II gene expression. We further examined whether PML-mediated Nrf2 regulation was related to alterations in ROS. To test this, we treated PML-knockdown HUVECs with *N*-acetyl cysteine (NAC) to eliminate ROS. We were unable to detect up-regulations of Nrf2 by PML knockdown in NAC-treated samples (Figure 4G), suggesting a requirement of ROS in PML-mediated regulation on Nrf2. Of note, Nrf2 levels were down-regulated

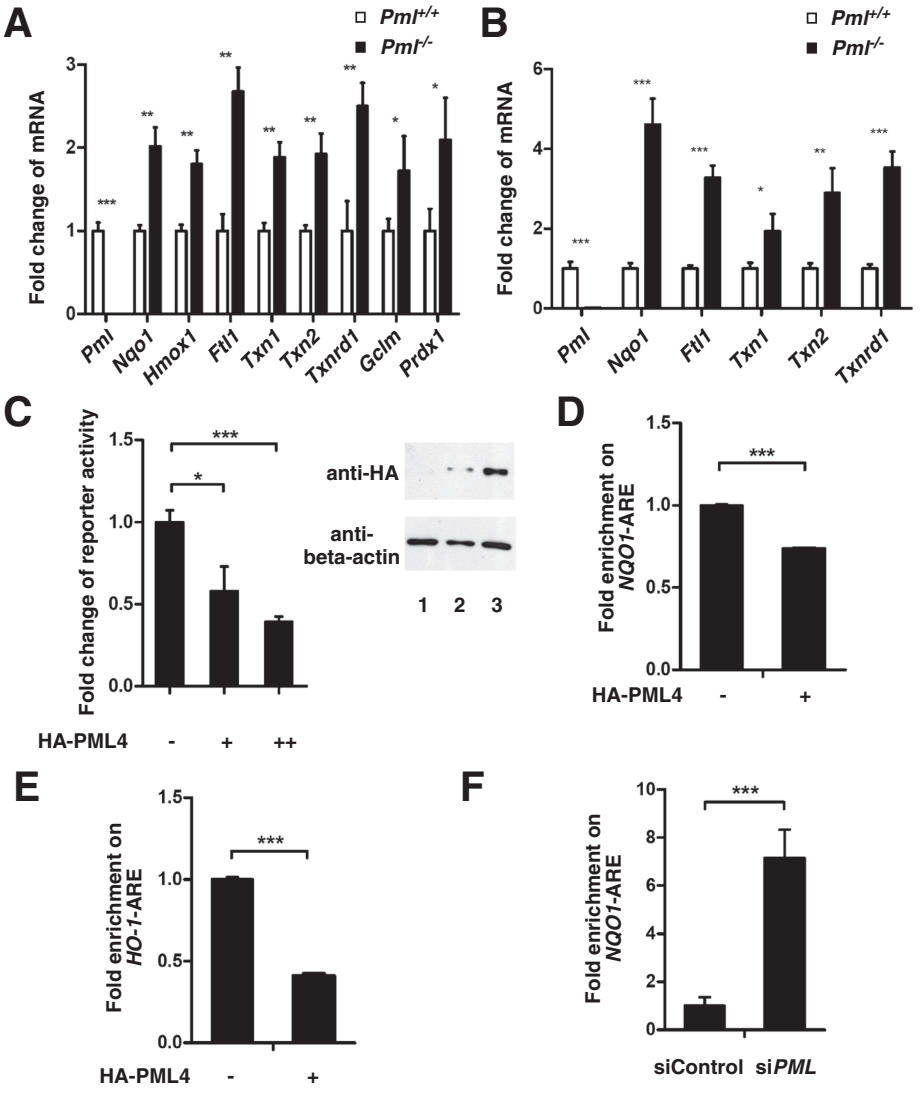

FIGURE 3: PML antagonizes transactivating activity of Nrf2. (A) qRT-PCR analysis of the mRNA levels of *Nrf2* target genes and *Pml* in $Pml^{+/+}$ and $Pml^{-/-}$ MEFs. Total RNA was prepared from $Pml^{+/+}$ and $Pml^{-/-}$ MEFs and reverse transcribed into cDNA, which was used as a template for qRT-PCR analysis. Values normalized to the amount of each mRNA in $Pml^{+/+}$ MEFs. Data presented as mean ± SD from triplicates. *$p < 0.05$; **$p < 0.01$; ***$p < 0.001$. (B) qRT-PCR analysis of mRNA levels of Nrf2 target genes and *Pml* in liver tissue isolated from $Pml^{+/+}$ and $Pml^{-/-}$ mice. Similar procedures were performed as in A. Data presented as mean ± SD from triplicates. *$p < 0.05$; **$p < 0.01$; ***$p < 0.001$. (C) Luciferase reporter assay and analysis of the effects of PML4 on an ARE-containing reporter. Different amounts of PML4 expression plasmid were transfected into CV-1 cells along with pNQO1-ARE reporter plasmid. At 24 h after transfection, the luciferase activity was measured in accordance with the instructions provided by the manufacturer. Data presented as mean ± SD from triplicates. *p < 0.05; ***$p < 0.001$. Cell extracts were analyzed by immunoblotting with the indicated antibodies. β-Actin was used as a loading control. (D) Effects of PML4 on the recruitment of Nrf2 to the *NQO1* promoter. HeLa cells were transfected with plasmids expressing HA-tagged PML4 and harvested for ChIP assays using anti-Nrf2 antibodies or anti-HA antibodies as a control. Percentages of amplified DNA amounts from precipitates as normalized to 10% of input are shown. Data presented as mean ± SD from triplicates. ***p < 0.001. (E) The effects of PML4 on the recruitment of Nrf2 to the *HO-1* promoter. Similar procedures were performed as in D. ***$p < 0.001$. (F) The effects of PML knockdown on the recruitment of Nrf2 to the *NQO1* promoter. HUVECs were transfected with a nontargeting siRNA or a PML targeting siRNA for 72 h and harvested for ChIP assays using anti-Nrf2 antibodies or anti-HA antibodies as a control. Percentages of amplified DNA amounts from precipitates as normalized to 10% of input are shown. ***$p < 0.001$.

by NAC treatment alone, likely due to the fact that NAC chelates ROS, which is required for Nrf2 activation.

The cysteine residues C212/213, C77/80, and C88/91 of PML have been reported to bind As_2O_3 and play an important role in As_2O_3-induced sumoylation and degradation (Jeanne *et al.*, 2010; Zhang *et al.*, 2010). PML may thus function as ROS scavenger via these cysteine residues. As such, it is possible that PML-mediated ROS decrease may also depend on these cysteines. To test this, we generated mutants C212/213A, C77/80A, and C88/91A and tested their effects on cellular ROS accumulation and their ability to decrease Nrf2 protein abundance. Figure 4H shows that these mutants behave similarly to the wild-type protein in reducing ROS accumulation and Nrf2 protein level. Taking the results together, we conclude that loss of PML results in complex II deficiency and ROS accumulation, which in turn induces nuclear Nrf2 accumulation and subsequently its target gene expression.

Sulforaphane alters subcellular distribution of PML

SFN reacts with the thiol groups of Keap1 and forms thioacyl adducts, thereby promoting dissociation of Keap1 from Nrf2 and subsequent induction of ARE-containing genes (Thimmulappa *et al.*, 2002; Hong *et al.*, 2005). To our surprise, SFN also induced PML protein levels in both a dose- and time-dependent manner in HUVECs (Figure 5, A and B). However, this regulation of SFN on PML was not at the transcriptional level (Supplemental Figure S4). We thus wondered whether the nuclear or cytoplasmic distributed PML was being affected by SFN. Unexpectedly, after SFN exposure, we found that nuclear PML was significantly reduced while cytoplasmic PML was concomitantly increased, all of which occurred at early time points accompanied by induction of Nrf2 in both the nucleus and the cytoplasm (Figure 5C). We also observed that slower-migrating bands of Nrf2 were more responsive to SFN treatment. Loss of nuclear PML upon SFN treatment was also confirmed by immunofluorescence microscopy. The treatment resulted in reduction in the number of PML NBs per cell and nuclear fluorescence intensity (Figure 5D). These observations suggest reverse correlation between Nrf2 and nuclear forms of PML, consistent with our previous observations (Figure 2). Our analysis thus far clearly shows that SFN induces accumulation of cytoplasmic PML while reducing nuclear PML.

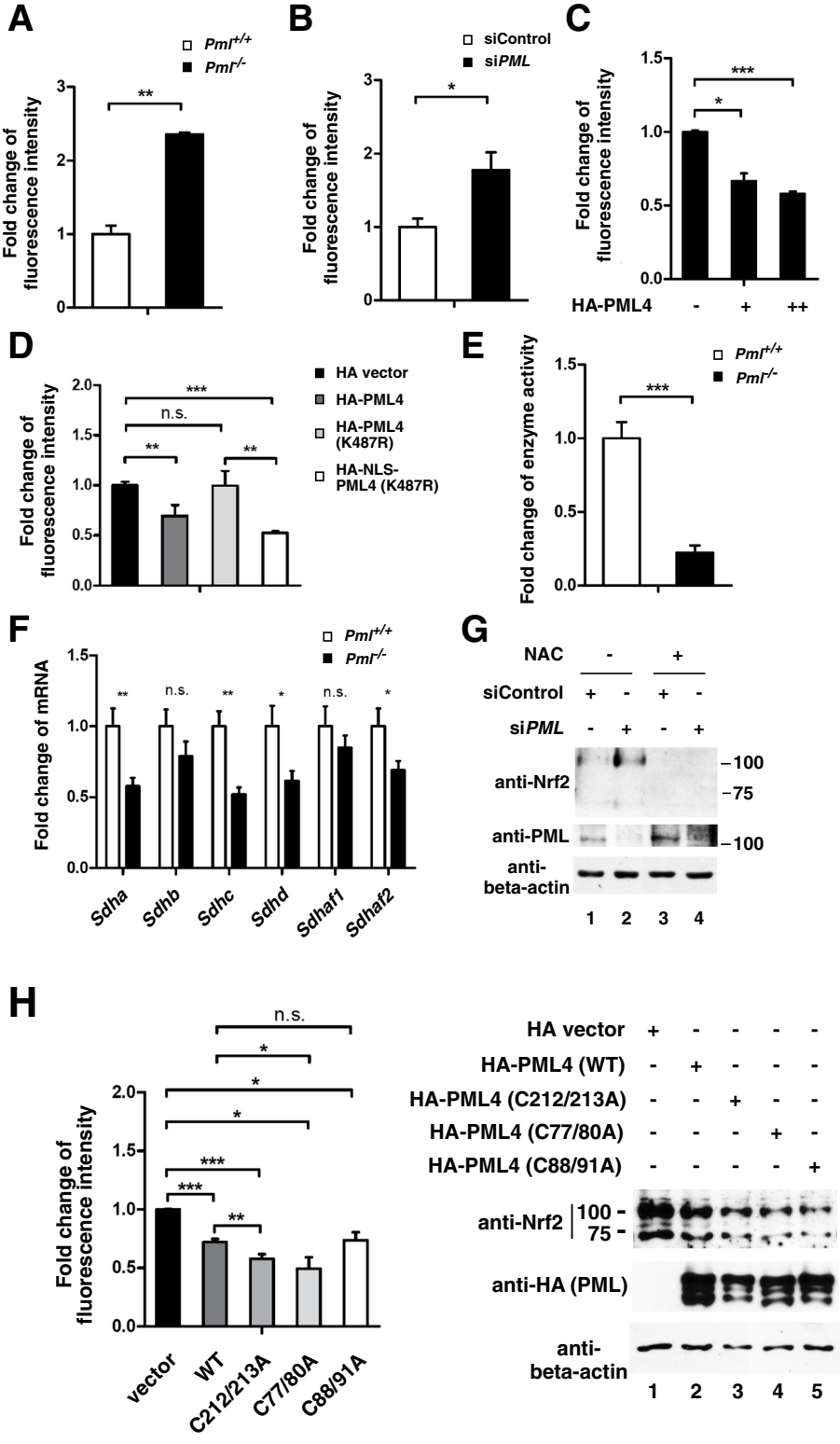

FIGURE 4: ROS accumulation due to mitochondrial defects accounts for PML-mediated Nrf2 regulations. (A) ROS accumulation in $Pml^{+/+}$ and $Pml^{-/-}$ MEFs. Equal numbers of $Pml^{+/+}$ and $Pml^{-/-}$ MEFs were cultured in a 96-well plate. The ROS levels were measured according to manufacturer's instruction. Data presented as mean ± SD from triplicates. $^{**}p < 0.01$. (B) ROS accumulation in PML-knockdown HUVECs. HUVECs were transfected with a nontargeting siRNA or a PML siRNA for 72 h, and ROS assays were carried out as in A. $^{*}p < 0.05$. (C) ROS accumulation in HeLa cells overexpressing PML4. Different amounts of an expression plasmid for PML4 were transfected into HeLa cells, and ROS assays were carried out as in A. $^{*}p < 0.05$; $^{***}p < 0.001$. (D) Effects of nuclear and cytoplasmic PML4 mutants on ROS accumulation in HeLa cells. Equal amounts of HA-tagged empty vector, wild-type PML, and cytoplasmic and nuclear PML mutants were transfected into HeLa cells, and ROS assays were carried out as in A. $^{**}p < 0.01$; $^{***}p < 0.001$; n.s., not significant. (E) Complex II enzyme activity assay of $Pml^{+/+}$ and $Pml^{-/-}$ mouse liver. The rate of enzyme activity was determined according to the manufacturer's instruction. $n = 3$ per group. $^{***}p < 0.001$; n, number of mice. (F) qRT-PCR analysis of mRNA levels of genes encoding components of complex II in liver tissue isolated from $Pml^{+/+}$ and $Pml^{-/-}$ mice. Fold change on mRNA abundance was normalized to the amount of each mRNA in $Pml^{+/+}$ tissue. $n = 3$ per group. $^{*}p < 0.05$; $^{**}p < 0.01$; n.s., not significant; n, number of mice. (G) Effects of NAC on Nrf2 protein accumulation in PML-knockdown HUVECs. HUVECs were transfected with a nontargeting siRNA or a PML siRNA for 48 h. Cells were then replated and treated with NAC for 24 h at 0 or 10 mM final concentration. Cell extracts were prepared and analyzed by immunoblotting with the indicated antibodies. β-Actin was used as a loading control. (H) The effects of C212/213A, C77/80A, and C88/91A mutations of PML on ROS accumulation and Nrf2 protein abundance. Equal amounts of HA-tagged empty vector, wild-type PML, and PML mutants were transfected into HeLa cells and split for ROS assays and immunoblotting. $^{*}p < 0.05$; $^{**}p < 0.01$; $^{***}p < 0.001$; n.s., not significant.

Keap1 binds to Nrf2 and promotes its proteasomal degradation (Itoh *et al.*, 1999). Our observation that PML deficiency induces accumulation of nuclear Nrf2 prompted us to further investigate whether Keap1 regulates PML protein accumulation. Using siRNA knockdown, we found that depletion of Keap1 had little or no effect on total PML protein abundance (Figure 5E). However, an increase in nuclear PML and a decrease in cytoplasmic PML were observed in Keap1-knockdown cells (Figure 5F). As expected, knockdown of Keap1 resulted in accumulation of nuclear Nrf2. We next addressed whether Keap1 plays a role in SFN-mediated regulation of PML. We found that SFN-induced nuclear reduction and cytoplasmic accumulation of PML were unchanged in both control and Keap1-knockdown cells (Figure 5G). Consistent with this observation, we found that SFN was capable of inducing total and cytoplasmic accumulation of PML in lung carcinoma cancer cell line A549 (Supplemental Figure S5), in which Keap1 is mutated, inactive, and expressed at an extremely low level (Singh *et al.*, 2006; Ohta *et al.*, 2008). Taken together, these data indicate that SFN-mediated regulation of PML is independent of Keap1 activity.

PML mediates multiple cellular functions of SFN

We demonstrated that loss of nuclear PML induces Nrf2 accumulation (Figure 2) by up-regulating ROS levels (Figure 4) and that SFN treatment results in a decrease in PML accumulation in the nucleus (Figure 5, C and D). We thus tested the hypothesis that SFN-mediated subcellular alteration of PML accounts for its ability to potentiate Nrf2 activity. Because it was previously shown that SFN treatments lead to ROS accumulation (Singh *et al.*, 2005; Choi *et al.*, 2008), we first tested whether PML is involved in this regulation by SFN. Using HUVECs transiently transfected with control or PML siRNA followed by SFN treatment, we were able to show that the SFN-mediated ROS increase was undetectable after PML knockdown (Figure 6A). This result indicates that SFN-dependent nuclear loss of PML contributes to ROS production and that Nrf2 is anticipated to be activated due to this elevation in ROS. As expected, when PML was knocked down, we found that the induction of Nrf2 by SFN was largely abolished at the protein level (Figure 6B) and that *NQO1* was no longer induced by SFN at the transcript level (Figure 6C). Moreover, SFN-induced recruitment of Nrf2 on the *NQO1*-ARE was drastically reduced in PML-knockdown cells (Figure 6D). These data indicate that SFN-induced Nrf2 activation is in part mediated by PML redistribution in a ROS-dependent manner.

We previously showed that PML is antiproliferative and antiangiogenic in ECs (Cheng *et al.*, 2012). In addition to its ability to activate Nrf2, SFN possesses antiproliferation and antiangiogenesis activity in ECs (Asakage *et al.*, 2006; Nishikawa *et al.*, 2010). However, the mechanism underlying these activities remains largely unknown. The observation that SFN affects the abundance and subcellular distribution of PML prompted us to investigate whether PML plays a role in SFN-mediated effects on proliferation and angiogenesis. To do so, we carried out proliferation assays in control and PML-knockdown HUVECs and observed that the proliferation rate was no longer decreased by SFN in PML-knockdown cells compared with control cells. In fact, it increased (Figure 7A). In addition, in scratch wound–healing assays, HUVECs were less affected by SFN when PML was knocked down (Figure 7B). Furthermore, we performed an in vitro capillary tube formation assay by analyzing the branch points of sprouting vessels, which represent the angiogenic capacity of ECs. We observed that the number of branch points per field was unchanged upon SFN treatment when PML was deficient but down-regulated in cells transfected with a control siRNA (Figure 7C). Taken together, our results unequivocally demonstrate that multiple pharmacological functions of SFN, including ROS elevation, Nrf2 activation, antiproliferation, antimigration, and antiangiogenesis, are all dependent on PML.

DISCUSSION

As stress-responsive structures, PML NBs are dynamic, and their size and components are constantly changing, depending on the cellular environment (Eskiw *et al.*, 2003; Dellaire and Bazett-Jones, 2004). These changes in PML levels and the composition of PML NBs are critical for the ability of cells to adapt to environmental cues and maintain cellular homeostasis. Indeed, several studies on the effects of As_2O_3 on PML and PML NBs have implied that PML is sensitive to redox disturbance (Jeanne *et al.*, 2010; Zhang *et al.*, 2010; Lallemand-Breitenbach *et al.*, 2012). In this study, loss of PML resulted in the inability of cells to control ROS levels and subsequent increases in ROS (Figure 4, A and B). Loss of Nrf2 also results in increased ROS (Frohlich *et al.*, 2008). Collectively these observations support a mechanism in which both PML and Nrf2 are parts of the same pathway critical for ROS homeostasis. As an alternative mechanism, it was proposed that PML promoted Nrf2 degradation in PML NBs by recruiting the E3 ubiquitin ligase RNF4 to sumoylated Nrf2 (Malloy *et al.*, 2013). However, based on our observations, Nrf2 is not subjected to sumoylation (Supplemental Figure S1, C and D), and we thus suggest Nrf2 may not be a RNF4 substrate. Paradoxically, RNF4 is also a PML E3 ubiquitin ligase (Lallemand-Breitenbach *et al.*, 2008; Tatham *et al.*, 2008; Weisshaar *et al.*, 2008; Percherancier *et al.*, 2009). If this model is correct, one would anticipate that loss of PML would result in decreased ROS due to increased Nrf2 in $Pml^{-/-}$ cells. However, our data unequivocally show that loss of PML increases cellular ROS levels.

Complex II is the only complex that participates in both citric acid cycle and mitochondrial oxidative phosphorylation. Although complex II has not generally been considered a major source of mitochondrial ROS, emerging evidence has demonstrated its indispensable role in ROS production (Paddenberg *et al.*, 2003; Calkins *et al.*, 2005; Ishii *et al.*, 2005; Guzy *et al.*, 2008). In this study, we identified PML as a critical regulator of mitochondrial function, in part by regulating complex II gene expression and activity. Because PML has been shown to regulate transcription factors, it is likely that nuclear PML controls the activity of transcription factors that directly or indirectly modulate promoter activity of complex II genes. The mechanism underlying PML's control of complex II gene expression warrants further investigation.

Mechanisms other than transcriptional dysregulation of genes encoding components of mitochondrial complex II likely contribute to the increased accumulation of ROS observed in PML-deficient cells. It is noteworthy that As_2O_3 directly binds to PML on C77/80 and C88/91, which leads to its enhanced sumoylation and ultimately degradation (Zhang *et al.*, 2010). Another study reported that C212/213 is also involved in As_2O_3 binding (Jeanne *et al.*, 2010). Thus PML may function as ROS scavenger via reactive cysteine residues. If this hypothesis is correct, one would anticipate that mutations of these cysteine residues would abolish the ability of PML to decrease ROS and subsequent Nrf2 accumulation. However, this is clearly not the case (Figure 4H). In addition, metabolic roles of PML that have recently been appreciated may link PML to ROS homeostasis in indirect ways. PML was shown to regulate PPAR signaling pathways and downstream events, including fatty acid metabolism (Kim *et al.*, 2011; Carracedo *et al.*, 2012; Ito *et al.*, 2012; Cheng *et al.*, 2013). Furthermore, our lab demonstrated that the energy sensor AMPK, which is also implicated in regulation of cellular ROS, is activated in $PML^{-/-}$ muscle and liver (Cheng *et al.*, 2013). Because some of the transcription factors regulated by PML are also involved in ROS regulation, we cannot rule out the possibility that PML controls cellular ROS levels indirectly through its regulation of transcription factors or energy sensors.

It has been proposed that SFN induces antioxidative responses by modifying reactive cysteine residues and subsequent inactivation of Keap1, therefore facilitating nuclear translocation of Nrf2 and transactivation of its antioxidant target genes (Thimmulappa *et al.*, 2002; Hong *et al.*, 2005). Indeed, the ability of SFN and oxidative stress to activate Nrf2 depends on Keap1 cysteine 151 (C151) (Zhang *et al.*, 2004). As such, one would predict that because SFN and ROS modify Keap1 C151, treatment of SFN in a ROS-enriched environment would not induce Nrf2 accumulation. Consistent with this notion, our data indicate that SFN has little or no effect on Nrf2 accumulation in PML-knockdown cells, in which elevated ROS was observed.

Of interest, whereas knockdown of Keap1 has little effect on total PML protein abundance, it significantly induces nuclear PML accumulation while reducing cytoplasmic PML abundance. However, Keap1 is not required for effects of SFN on the subcellular distribution of PML. These results indicate that SFN and knockdown

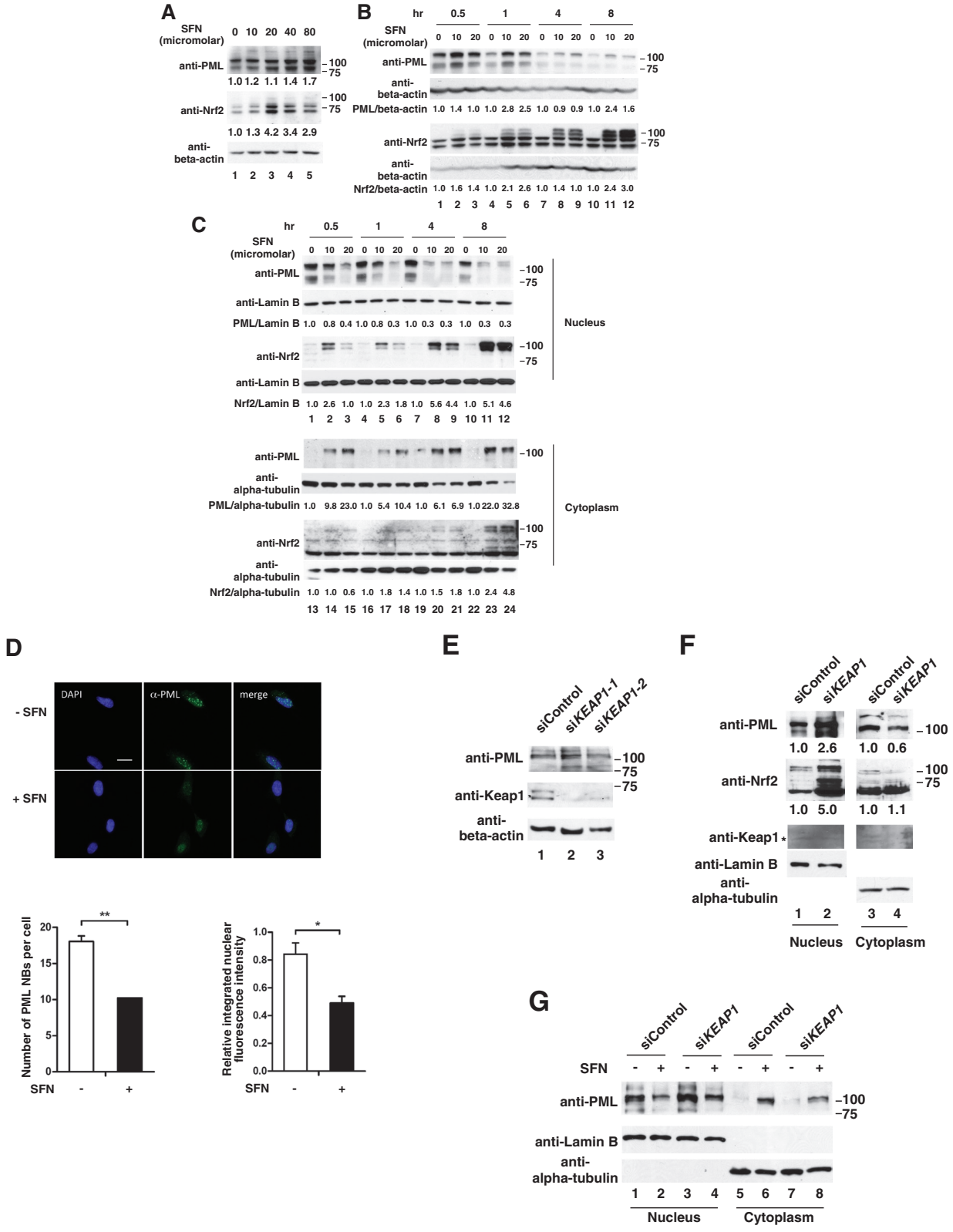

FIGURE 5: The effects of SFN on abundance and subcellular distribution of PML. (A) Immunoblotting analysis of HUVECs treated with different concentrations of SFN. HUVECs were treated with SFN for 1 h at 0, 10, 20, 40, or 80 μM final concentration. Cell extracts were analyzed by immunoblotting with the indicated antibodies. β-Actin was used as loading control. (B) Immunoblotting analysis of HUVECs treated with SFN. HUVECs were treated with vehicle control (DMSO) or SFN at 10 or 20 μM for 0.5, 1, 4, or 8 h. Relative intensities of the bands are normalized to both loading control and DMSO within each time point. (C) Subcellular fractionation and immunoblotting analysis of HUVECs treated with SFN. HUVECs were treated with vehicle control (DMSO) or SFN at 10 or 20 μM for 0.5, 1, 4, or 8 h. Nuclear and cytoplasmic fractions prepared were subjected to immunoblotting analysis with the indicated antibodies. Lamin B and

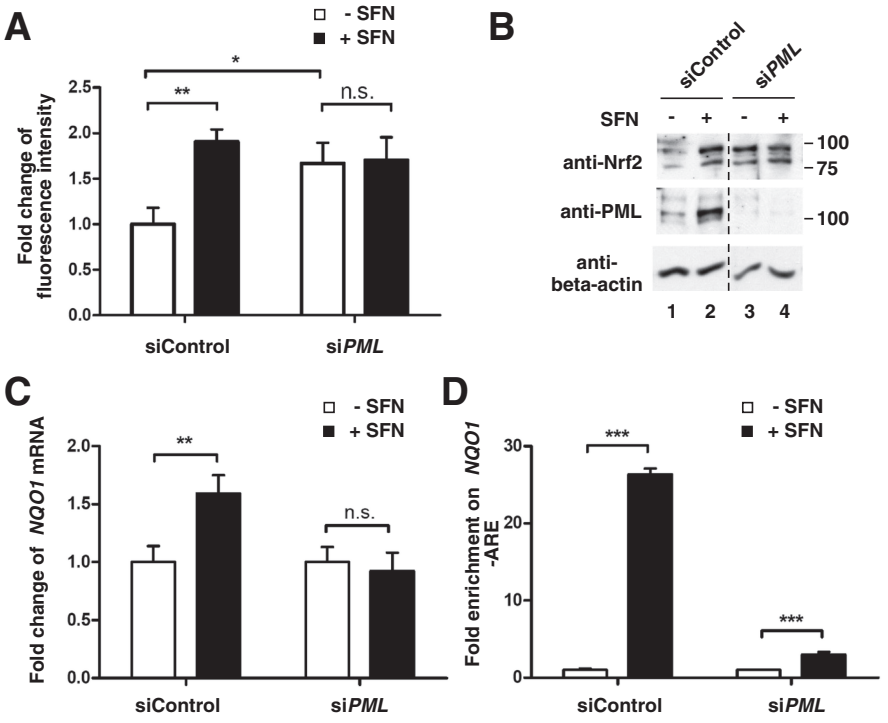

FIGURE 6: SFN-mediated Nrf2 activation is PML dependent. (A) ROS accumulation in PML knockdown HUVECs. HUVECs were transfected with a nontargeting siRNA or a PML siRNA for 72 h. Equal number of HUVECs were replated in a 96-well plate and treated with vehicle control (DMSO) or SFN at 40 μM for 1 h. The ROS level was measured according to the manufacturer's instruction. Data presented as mean ± SD from triplicates. *$p < 0.05$; **$p < 0.01$; n.s., not significant. (B) Immunoblotting analysis of PML-knockdown HUVECs treated with SFN. HUVECs were transfected with a nontargeting siRNA or a PML targeting siRNA for 48 h. Cells were then replated and treated with vehicle control (DMSO) or SFN at 20 μM for 1 h. Cell extracts were analyzed by immunoblotting with the indicated antibodies. β-Actin was used as a loading control. Dividing line marks edges of different parts of the same gel. (C) qRT-PCR analysis of the mRNA levels of *NQO1* in PML-knockdown HUVECs with SFN treatment. HUVECs were subjected to PML knockdown and SFN treatment as in B and harvested for qRT-PCR. Fold change of *NQO1* mRNA was normalized to that in vehicle-treated cells within each group. Data presented as mean ± SD from triplicates. **$p < 0.01$; n.s., not significant. (D) The effects of PML on the recruitment of Nrf2 to the *NQO1* promoter after SFN treatment. HUVECs were subjected to PML knockdown and SFN treatment as in B and harvested for ChIP assays using anti-Nrf2 antibodies or anti-HA antibodies as a control. Percentages of amplified DNA amounts from precipitates as normalized to 10% of input are shown. Data presented as mean ± SD from triplicates. ***$p < 0.001$.

PML protein accumulation is regulated by SFN in a dose- and time-dependent manner in HUVECs. At 1 h, we observed a twofold to threefold increase in PML protein levels without changes in PML mRNA. Of interest, this induction is accompanied by significant loss of nuclear PML and accumulation of cytoplasmic PML. These effects were observed as early as 0.5 h after SFN administration. Further investigation is needed to dissect the mechanism by which SFN regulates PML accumulation and subcellular distribution.

Using an siRNA knockdown approach (Supplemental Figure S1) and subcellular fractionation (Figures 2 and 5), we demonstrated that in unstimulated HUVECs, a major Nrf2 isoform predominantly localizes in the cytoplasm and migrates faster than the 75-kDa marker. The predicted molecular weight of Nrf2 is 68 kDa, so we assume that the fastest-migrating species is the unmodified Nrf2. In contrast, SFN induced accumulation of nuclear Nrf2, which migrated close to the 100-kDa marker. We speculate that the slower migration (100 kDa) of the nuclear Nrf2 species is due to a posttranslational modification. Indeed, phosphatase treatment resulted in the disappearance of the slowest-migrating Nrf2 species (Supplemental Figure S1B), which is consistent with previous reports suggesting that Nrf2 is phosphorylated by PKC, GSK-3β, CK2, and JNK (Huang *et al.*, 2002; Salazar *et al.*, 2006; Xu *et al.*, 2006; Apopa *et al.*, 2008).

The antiangiogenesis activity of SFN has been attributed to its ability to inhibit EC proliferation (Jackson *et al.*, 2007) and vascular endothelial growth factor or transcription factors such as HIF-1a and c-Myc (Bertl *et al.*, 2006). We are the first group to establish SFN-induced cytoplasmic accumulation of PML as an important action in its antiangiogenic activity. Moreover, because PML NBs possess well-established proapoptotic and antiproliferative properties, recent studies have started to focus on the tumor suppressor activity of cytoplasmic PML. One study showed that cytoplasmic PML is able to activate Ca^{2+} release from endoplasmic reticulum, which contributes to the apoptotic property of PML (Giorgi *et al.*, 2010). Another study of Keap1 regulate the subcellular distribution of PML through distinct mechanisms. Several studies reported that NF-κB and histone deacetylases are also SFN targets (Heiss *et al.*, 2001; Myzak *et al.*, 2004). These data further provide alternative pathways by which SFN promotes its antioxidative activity. Our data show that

α-tubulin were used as loading controls for nuclear and cytoplasmic fractions, respectively. Relative intensities of the bands are normalized to both loading control and DMSO within each time point. (D) Immunofluorescence analysis of HUVECs treated with SFN. HUVECs were treated with vehicle control (DMSO) or SFN at 10 μM for 1 h. Cells were immunostained with anti-PML antibodies, and images were taken on a fluorescence microscope. Nuclei were stained with DAPI, and PML NBs are shown in green. Statistical analysis of the PML NB number and nuclear fluorescence intensity. $n > 150$ per group. *$p < 0.05$; **$p < 0.01$; *n*, number of cells. Scale bar, 20 μm. (E) The effects of Keap1 knockdown on PML protein abundance in HUVECs. HUVECs were transfected with a nontargeting siRNA or two independent Keap1 siRNAs for 72 h. Cell extracts were analyzed by immunoblotting with the indicated antibodies. (F) The effects of Keap1 knockdown on subcellular distribution of PML in HUVECs. HUVECs were subjected to Keap1 knockdown as in E and followed by subcellular fractionation as in C. Asterisk, nonspecific band. (G) Immunoblotting analysis of Keap1-knockdown HUVECs treated with SFN. HUVECs were transfected with a nontargeting siRNA or Keap1 siRNA for 72 h and replated, treated with vehicle control (DMSO) or SFN at 10 μM for 1 h, and harvested for subcellular fractionation as in C.

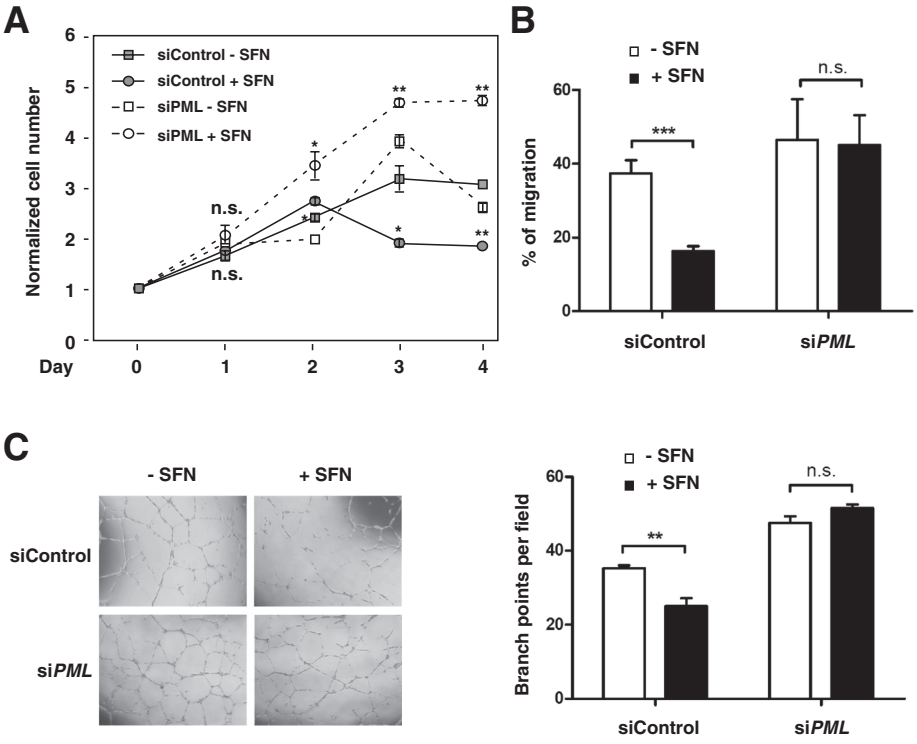

FIGURE 7: PML is required for SFN-mediated antiproliferation, antimigration, and antiangiogenesis activity. (A) The effects of PML knockdown on proliferation of SFN-treated HUVECs. HUVECs were transfected with a nontargeting siRNA or a PML siRNA for 48 h. Cells were then replated and treated with vehicle control (DMSO) or SFN at 10 μM for 3 h. A cell proliferation assay was performed in accordance with the instructions provided by the manufacturer. Cell numbers were determined at 0, 24, 48, and 72 h and normalized to the 0-h group. Data presented as mean ± SEM from triplicates. *$p < 0.05$; **$p < 0.01$; n.s., not significant. (B) The effects of PML knockdown on migration of SFN-treated HUVECs. HUVECs were transfected with a nontargeting siRNA or a PML siRNA for 48 h. Cells were then replated and treated with vehicle control (DMSO) or SFN at 10 μM for 4 h. Wounds were generated using a pipette tip, and images were taken at 0 and 12 h afterward. Wound widths were measured and are shown as percentages of migration. $n = 6$ per group. Data presented as mean ± SD from triplicates.***$p < 0.001$; n.s., not significant; *n*, number of fields. (C) The effects of PML knockdown on capillary tube formation of SFN-treated HUVECs. HUVECs were subjected to PML knockdown and SFN treatment as in B. In vitro capillary tube formation assays were performed according to manufacturer's instructions. Images were taken 21 h after HUVECs were seeded on Matrigel. Statistical analysis was performed by counting branch points per field. $n = 5$ per group. Data presented as mean ± SEM from triplicates. **$p < 0.01$; n.s., not significant; *n*, number of fields.

suggested that cytoplasmic PML expression is induced by transforming growth factor β (TGFβ) and plays an essential role in TGFβ signaling–mediated growth arrest of cells (Lin *et al.*, 2004). Thus one should not equate all of the antiproliferative, antiangiogenic, and proapoptotic activity of SFN to decreases in nuclear PML and reduced number of PML NBs. It is possible that SFN cellular activity is mediated by increased cytoplasmic PML. The specific functions of nuclear and cytoplasmic PML isoforms and differentially modified PMLs in SFN-treated cells require further elucidation. Nonetheless, our findings that PML is indispensable for SFN-mediated ROS generation, Nrf2 activation, antiproliferation, antimigration, and antiangiogenesis activity provide a novel and plausible mechanism for the mysterious chemopreventive property of SFN.

In summary, PML participates in oxidative responses in part by controlling the Nrf2-dependent antioxidative pathway. The idea that PML serves as a mediator for multiple SFN actions opens up the significance of its involvement in antioxidative responses. Our study provides additional insights into the mechanisms regulating ROS homeostasis and implications in therapeutic designs for cancer treatments.

MATERIALS AND METHODS

Cell culture and medium

HUVECs (C2519A; Lonza, Basel, Switzerland) were grown in Endothelial Cell Growth Medium-2 (CC-4176; Lonza) supplemented with fetal bovine serum (FBS) and growth factors (Lonza). Cells of fewer than five passages were used in this study. HeLa, CV-1, and A549 cells were maintained in 1× DMEM with 4.5 g/liter glucose, L-glutamine, and sodium pyruvate supplemented with 10% charcoal-stripped FBS (F0926; Sigma-Aldrich, St. Louis, MO) and 100× Penicillin-Streptomycin Solution (30-002-CI; Mediatech, Manassas, VA). MEFs were grown in the same medium as HeLa and CV-1 cells except supplemented with 55°C heat-inactivated FBS. All cells were maintained in a humidified 37°C, 5% CO_2 incubator.

Chemicals and antibodies

SFN (S4441; Sigma-Aldrich) and CHX (01810; Sigma-Aldrich) were dissolved in dimethyl sulfoxide (DMSO; D128-1; Thermo Fisher Scientific, Waltham, MA), which was also used as a vehicle control. All SFN treatments in HUVECs and A549 cells were performed in basal medium with no supplements. NAC (A8199; Sigma-Aldrich) was dissolved in double-distilled water. The commercial antibodies used in this study were anti-human PML (sc-562; Santa Cruz Biotechnology, Dallas, TX), anti-mouse PML (MAB3738; EMD Millipore, Billerica, MA), anti-human PML peptide antibody generated against sequence PSTSKAV-S(PO3)-PPHLDGPP (Affinity BioReagents, Golden, CO), anti-Nrf2 (sc-13032; Santa Cruz Biotechnology), anti-NQO1 (ab28947; Abcam, Cambridge, MA), anti-Keap1 (sc-15246; Santa Cruz Biotechnology), anti-hemagglutinin (HA; sc-7392; Santa Cruz Biotechnology; 12013819001; Roche, San Francisco, CA), anti-FLAG (F3165; Sigma-Aldrich), anti–green fluorescent protein (GFP; sc-9996; Santa Cruz Biotechnology), anti–β-actin (A5441; Sigma-Aldrich), anti–lamin B (sc-6216; sc-365962; Santa Cruz Biotechnology), anti–α-tubulin (T5168; Sigma-Aldrich); anti-mouse immunoglobulin G (IgG) conjugated with horseradish peroxidase (HRP; sc-2005; Santa Cruz Biotechnology), anti-rabbit IgG conjugated with HRP (12-348; EMD Millipore), anti-goat IgG conjugated with HRP (sc-2033; Santa Cruz Biotechnology); Alexa Fluor 488 μm goat anti-rabbit (A-11008; Life Technologies, Grand Island, NY), Alexa Fluor 488 μm goat anti-mouse (A-11001; Life Technologies), and Alexa Fluor 594 μm goat anti-mouse (A-11005; Life Technologies).

siRNA transfection

HUVECs were grown to 60% confluency and then treated with either a nontargeting small siRNA oligonucleotide (D-001810-01-50;

Dharmacon, Lafayette, CO) or siRNAs against PML (J-006547-05 and J-006547-07; Dharmacon) or Nrf2 (J-003755-10 and J-003755-11; Dharmacon) or Keap1 (J-012453-05 and J-012453-06; Dharmacon) according to the manufacturer's protocol using DharmaFECT1 (T-2001; Thermo Fisher Scientific).

Microarray analysis

Procedures for analyzing microarray data have been published elsewhere (Cheng *et al.*, 2012). Briefly, HUVECs were transiently transfected with control siRNA or two different PML siRNAs (si*PML*-1 and si*PML*-2) for 72 h, followed by total RNA extraction using PrepEase RNA spin kit (78766; USB/Affymetrix, Cleveland, OH). The microarray hybridization was carried out by the Genomics Core at Cleveland Clinic Foundation, and HumanRef-8_V2_0_R0_11223162_A chip (Illumina, San Diego, CA) was used. Each sample had technical duplicates. All statistical analysis was done in R/Bioconductor. The raw data were transformed by the Variance-Stabilizing Transformation method and then normalized using the Robust Spline Normalization package. The significantly changed gene list was retrieved by a general linear model and empirical Bayes method through the Linear Models for Microarray Data (limma) package with the false discovery rate adjusted by Benjamini and Hochberg's method. The data were represented in a heat map with the row *z*-score mapped to a green/black/red color scheme.

Mouse embryonic fibroblast and liver tissue isolation

$Pml^{+/+}$ and $Pml^{-/-}$ mice were maintained in the $129^{S1/SvImJ}$ background in the Health Science Animal Facility of Case Western Reserve University. MEFs were isolated from pregnant female mice 13.5 d postcoitum. Genotyping was performed by PCR using extracted DNA from head tissue of embryos. MEFs with $Pml^{+/+}$ and $Pml^{-/-}$ background were used in this study. Liver tissue was isolated from $Pml^{+/+}$ and $Pml^{-/-}$ mice killed with CO_2.

Plasmid construction and transfection

pCMX-HA-PML1, pCMX-HA-PML4, and pCMX-GFP were previously described (Reineke *et al.*, 2008). pCMX-HA-PML4-K487R, pCMX-ATG-NLS-HA-PML4-K487R, pCMX-ATG-NLS-HA-PML4, pCMX-HA-PML4-C212/213A, pCMX-HA-PML4-C77/80A, pCMX-HA-PML4-C88/91A, and pCMX-FLAG-Nrf2 were generated by PCR and site-directed mutagenesis. All constructs were verified by DNA sequencing. The primer sequences are listed in Supplemental Table S1. HeLa cells, HUVECs, and CV-1 cells were transfected with plasmids using Lipofectamine 2000 (P/N 52887; Life Technologies) following the manufacturer's protocol. The amount of plasmid transfected in each sample was kept constant by adding vector controls.

Immunoblotting

Whole-cell extracts were prepared by incubating harvested cells for 30 min in radioimmune precipitation assay buffer (1× phosphate-buffered saline [PBS], 1% Nonidet P-40, 0.5% sodium deoxycholate, and 0.1% SDS) supplemented with protease inhibitors. Insoluble components were removed by centrifugation at 13,000 rpm for 15 min at 4°C, and whole-cell extracts were subjected to SDS–PAGE. Proteins were transferred to polyvinylidene fluoride membranes (IPVH00010; EMD Millipore), and products were visualized by immunoblotting. Membranes were blocked in 10% nonfat milk in 1× PBS with 0.1% Tween-20 (PBST) for 30 min at room temperature, and primary antibodies were added in 5% milk/PBST solution for 2–3 h at room temperature or overnight at 4°C. Membranes were then washed with PBST, and secondary antibodies were added in 5% milk/PBST solution for 30 min at room temperature. After three washes with PBST, detection was performed using ECL detection kits (34080; Thermo Fisher Scientific; K-12045-D50; Laboratory Products Sales, Rochester, NY). Intensities of the bands were quantified by ImageJ, version 1.46r (National Institutes of Health, Bethesda, MD).

Coimmunoprecipitation

Coimmunoprecipitation was performed according to our published protocol (Su *et al.*, 2013). Briefly, whole-cell extracts were prepared by incubating harvested cells for 30 min in NETN buffer (20 mM Tris-HCl, pH 8.0, 100 mM NaCl, 1 mM EDTA, 10% glycerol, 1 mM dithiothreitol, 0.1% Nonidet P-40) supplemented with protease inhibitors and *N*-ethylmaleimide, followed by sonication and centrifugation. Immunoprecipitations were carried out using anti–FLAG antibody–conjugated agarose (F2426; Sigma-Aldrich) overnight at 4°C. Beads were washed with NETN buffer five times, and immunoprecipitates were subjected to SDS–PAGE and immunoblotting.

Subcellular fractionation

Subcellular fractionations of MEFs, HUVECs, and HeLa and A549 cells were carried out according to a published protocol (Li *et al.*, 2004). Briefly, harvested cell pellets were resuspended and lysed in cytoplasmic lysis buffer and incubated for 15 min on ice. Cytoplasmic fractions were acquired by centrifugation at 3000 rpm for 5 min at 4°C. Nuclear pellets were washed once with cytoplasmic lysis buffer, followed by centrifugation at 3000 rpm for 5 min at 4°C. Nuclear lysis buffer was then added to nuclear pellets, and the mixture was incubated on ice for 30 min with occasional stirring. Nuclear fractions were acquired by centrifugation at 3000 rpm for 15 min at 4°C. Both nuclear and cytoplasmic fractions were subjected to SDS–PAGE and immunoblotting analysis.

Immunofluorescence microscopy

Immunofluorescence microscopy was performed as previously described (Gao *et al.*, 2008). Briefly, MEFs, HUVECs, or HeLa cells, plated on glass coverslips in a 12-well plate, were transfected with the indicated plasmids or treated with SFN with the indicated doses. The cells were fixed in 3.7% paraformaldehyde by incubating for 30 min at room temperature and washed three times with 1× PBS. Permeabilization was performed by incubating cells with 1× PBS supplemented with 1% Triton X-100 and 10% goat serum for 10 min. The plate was covered to avoid light after this step. Cells were then washed with 1× PBS three times and blocked in 1× PBS supplemented with 0.1% Tween-20 and 10% goat serum for 1 h. Primary antibodies were added to the cells for 2 h, followed by three washes with 1× PBS. Secondary antibodies conjugated with Alexa Fluor were added for 30 min, followed by three washes with 1× PBS. Coverslips were mounted on slides using Vectashield mounting medium with 4′,6-diamidino-2-phenylindole (DAPI; H-1200; Vector Laboratories, Burlingame, CA) to visualize nuclei. Images were captured by a Leica immunofluorescence microscope (Leica, Wetzlar, Germany) using a 40× lens. Images were captured by a computer connected with a digital camera at room temperature. All images were taken under same microscope settings. Intensity of integrated nuclear fluorescence was determined by ImageJ, version 1.46r.

Total RNA extraction, reverse transcription PCR, and quantitative real-time PCR

Cells or liver tissue was harvested and total RNAs were extracted using PrepEase RNA spin kit (78766; USB/Affymetrix) and quantified by A260/A280 spectrometry. Total RNA was used for reverse

transcription PCR. The cDNA pool was generated from each RNA sample using the iScript Reverse Transcription Supermix kit (170-8841; Bio-Rad Laboratories, Hercules, CA) with a PCR program of 25°C for 5 min, 42°C for 30 min, and 85°C for 5 min. Quantitative real-time PCR (qRT-PCR) was performed using an iCycler (Bio-Rad Laboratories) platform with 2X iQ SYBR Green Supermix (170-8880; Bio-Rad Laboratories). The PCR program was 1 cycle of 95°C for 3 min, 50 cycles of 94°C for 15 s, 57°C for 20 s, and 72°C for 30 s. The relative abundance of an mRNA was normalized to the level of 18S rRNA and is presented as the mean ± SD from three experiments. The primer sequences are listed in Supplemental Table S1.

Luciferase reporter assay

The luciferase reporter assay was performed according to a published protocol (Cheng and Kao, 2009). Briefly, CV-1 cells were cotransfected with pNQO1-ARE-Luc (gift from Masayuki Yamamoto, Tohoku University, Sendai, Japan; Kang *et al.*, 2004) and pCMX-β-gal, with or without pCMX-HA-PML4. Cells were harvested 24 h after transfection; luciferase and β-galactosidase activities were measured with kits according to the manufacturer's protocol (E1501; Promega, Madison, WI). Luciferase activity was normalized to β-gal activity, and fold change is presented as the mean ± SD from three experiments. Unpaired two-tail *t* tests were performed to determine significance.

ChIP assay

The ChIP assay was performed according to our published protocol (Cheng and Kao, 2009). Briefly, HeLa cells were transfected with an empty vector or HA-tagged PML4 for 48 h, and HUVECs were transfected with control siRNA or siRNA targeting PML for 72 h. Anti-Nrf2 antibodies were used for immunoprecipitation, with anti-HA antibodies as a control. qRT-PCR was performed to quantify retrieved DNAs, and primer sequences are listed in Supplemental Table S1. The results were calculated from three independent qRT-PCR experiments and are presented as the mean ± SD of the relative fold enrichment as the percentage of 10% input signal. Unpaired two-tail *t* tests were performed to determine significance.

ROS assay

The ROS assay was performed using the OxiSelect Intracellular ROS Assay Kit (STA-342; Cell Biolabs, San Diego, CA). Briefly, $Pml^{+/+}$ and $Pml^{-/-}$ MEFs, PML-knockdown HUVECs, or transfected HeLa cells were cultured in a 96-well plate. Cell-permeable fluorogenic probe 2′,7′-dichlorodihydrofluorescin diacetate was added to wells, followed by 1-h incubation in a cell incubator. The assay was terminated by adding cell lysis buffer and incubating for 5 min. Fluorescence intensities were quantified by a SpectraMax M2 plate reader (Molecular Devices, Sunnyvale, CA) at 480/530 nm with 530-nm cutoff. All samples were prepared in triplicate and data are presented as the mean ± SD from three experiments. Unpaired two-tail *t* tests were performed to determine significance.

Complex II enzyme activity assay

The complex II enzyme activity assay was performed using the Complex II Enzyme Activity Microplate Assay Kit (MS241; MitoSciences, Eugene, OR). Briefly, liver homogenates with equal amount of protein were prepared with buffers provided in the kit and loaded to the enzyme-linked immunosorbent assay plate coated with anti–complex II antibody in triplicate. After 2 h of incubation at room temperature, the plate was washed two times; enzyme substrates succinate and ubiquinone were added, together with the blue ubiquinol substrate 2,6-dichlorophenolindophenol and incubated for 30 min. The kinetics of enzyme activity was measured for 2 h at 1-min intervals by monitoring the OD_{600} absorbance using a SpectraMax M2 plate reader.

Cell proliferation assay

The cell proliferation assay was performed using the CellTiter 96 AQueous One Solution Cell Proliferation Assay Kit (G3580; Promega). Briefly, HUVECs were transfected with either control siRNA or PML siRNA for 48 h. Before the assay, cells were replated and pretreated with SFN for 3 h at 0 or 10 μM final concentration and seeded to five 96-well plates in triplicate with equal cell number (1×10^3 cells/well). After 0, 24, 48, 72, and 96 h, cells were treated with reagents provided in the kit, and DNA content within each well was measured using a SpectraMax M2 plate reader at A_{490}. Cell numbers were normalized to day 0 and are presented as the mean ± SD. Unpaired two-tail *t* tests were performed to determine significance.

Wound-healing assay

HUVECs were transfected with either control siRNA or PML siRNA for 48 h and replated on a 12-well plate in duplicate with equal cell number (6×10^4 cells/well). Before the wound-healing assay, cells were pretreated with SFN for 4 h at 0 or 10 μM final concentration. Wounds were then generated in each well using a 200-μl pipette tip. Images were taken at 0 and 12 h using a Leica Wetzlar microscope. Wound widths were measured by ImageJ and are presented as percentage of width difference between 0 and 12 h divided by width at 0 h ($n = 6$). Percentages of migration are presented as the mean ± SD, and unpaired two-tail *t* tests were performed to determine significance.

In vitro capillary tube formation assay

Capillary tube formation assays were performed using an *In Vitro* Angiogenesis Assay Kit (ECM625; EMD Millipore). Briefly, HUVECs were transfected with control siRNA or PML siRNA for 48 h. Before the assay, cells were replated and pretreated with or without SFN for 4 h at 0 or 10 μM final concentration and then seeded to a 96-well plate coated with Matrigel with equal cell number (1×10^3 cells/well). Images were taken after 3, 7, and 21 h in randomly picked fields ($n = 5$) using a Leica Wetzlar microscope. Statistical analysis and images presented are based on branch point counts in images taken at 21 h. The branch points presented are the mean ± SD, and unpaired two-tail *t* tests were performed to determine significance.

ACKNOWLEDGMENTS

We thank David Samols for his comments on the manuscript and Masayuki Yamamoto for providing us with the pNQO1-ARE reporter plasmid. This work was supported by National Institutes of Health Grants RO1 DK078965 and HL093269 to H.-Y.K.

REFERENCES

Andersen JK (2004). Oxidative stress in neurodegeneration: cause or consequence? Nat Med 10, S18–S25.

Apopa PL, He X, Ma Q (2008). Phosphorylation of Nrf2 in the transcription activation domain by casein kinase 2 (CK2) is critical for the nuclear translocation and transcription activation function of Nrf2 in IMR-32 neuroblastoma cells. J Biochem Mol Toxicol 22, 63–76.

Asakage M *et al.* (2006). Sulforaphane induces inhibition of human umbilical vein endothelial cells proliferation by apoptosis. Angiogenesis 9, 83–91.

Bertl E, Bartsch H, Gerhauser C (2006). Inhibition of angiogenesis and endothelial cell functions are novel sulforaphane-mediated mechanisms in chemoprevention. Mol Cancer Ther 5, 575–585.

Calkins MJ, Jakel RJ, Johnson DA, Chan K, Kan YW, Johnson JA (2005). Protection from mitochondrial complex II inhibition in vitro and in vivo by Nrf2-mediated transcription. Proc Natl Acad Sci USA 102, 244–249.

Carracedo A *et al.* (2012). A metabolic prosurvival role for PML in breast cancer. Eur J Clin Invest 122, 3088–3100.
Cheng X, Guo S, Liu Y, Chu H, Hakimi P, Berger NA, Hanson RW, Kao HY (2013). Ablation of promyelocytic leukemia protein (PML) re-patterns energy balance and protects mice from obesity induced by a western diet. J Biol Chem 288, 29746–29759.
Cheng X, Kao HY (2009). G protein pathway suppressor 2 (GPS2) is a transcriptional corepressor important for estrogen receptor alpha-mediated transcriptional regulation. J Biol Chem 284, 36395–36404.
Cheng X, Liu Y, Chu H, Kao HY (2012). Promyelocytic leukemia protein (PML) regulates endothelial cell network formation and migration in response to tumor necrosis factor alpha (TNFalpha) and interferon alpha (IFNalpha). J Biol Chem 287, 23356–23367.
Choi WY, Choi BT, Lee WH, Choi YH (2008). Sulforaphane generates reactive oxygen species leading to mitochondrial perturbation for apoptosis in human leukemia U937 cells. Biomed Pharmacother 62, 637–644.
Dellaire G, Bazett-Jones DP (2004). PML nuclear bodies: dynamic sensors of DNA damage and cellular stress. BioEssays 26, 963–977.
de The H, Le Bras M, Lallemand-Breitenbach V (2012). The cell biology of disease: acute promyelocytic leukemia, arsenic, PML bodies. J Cell Biol 198, 11–21.
Eskiw CH, Dellaire G, Mymryk JS, Bazett-Jones DP (2003). Size, position and dynamic behavior of PML nuclear bodies following cell stress as a paradigm for supramolecular trafficking and assembly. J Cell Sci 116, 4455–4466.
Farout L, Friguet B (2006). Proteasome function in aging and oxidative stress: implications in protein maintenance failure. Antiox Redox Signal 8, 205–216.
Fimognari C, Nusse M, Cesari R, Iori R, Cantelli-Forti G, Hrelia P (2002). Growth inhibition, cell-cycle arrest and apoptosis in human T-cell leukemia by the isothiocyanate sulforaphane. Carcinogenesis 23, 581–586.
Frohlich DA, McCabe MT, Arnold RS, Day ML (2008). The role of Nrf2 in increased reactive oxygen species and DNA damage in prostate tumorigenesis. Oncogene 27, 4353–4362.
Gamet-Payrastre L, Li P, Lumeau S, Cassar G, Dupont MA, Chevolleau S, Gasc N, Tulliez J, Terce F (2000). Sulforaphane, a naturally occurring isothiocyanate, induces cell cycle arrest and apoptosis in HT29 human colon cancer cells. Cancer Res 60, 1426–1433.
Gao C, Cheng X, Lam M, Liu Y, Liu Q, Chang KS, Kao HY (2008). Signal-dependent regulation of transcription by histone deacetylase 7 involves recruitment to promyelocytic leukemia protein nuclear bodies. Mol Biol Cell 19, 3020–3027.
Giorgi C *et al.* (2010). PML regulates apoptosis at endoplasmic reticulum by modulating calcium release. Science 330, 1247–1251.
Guzy RD, Sharma B, Bell E, Chandel NS, Schumacker PT (2008). Loss of the SdhB, but Not the SdhA, subunit of complex II triggers reactive oxygen species-dependent hypoxia-inducible factor activation and tumorigenesis. Mol Cell Biol 28, 718–731.
Han Y *et al.* (2010). SENP3-mediated de-conjugation of SUMO2/3 from promyelocytic leukemia is correlated with accelerated cell proliferation under mild oxidative stress. J Biol Chem 285, 12906–12915.
Heiss E, Herhaus C, Klimo K, Bartsch H, Gerhauser C (2001). Nuclear factor kappa B is a molecular target for sulforaphane-mediated anti-inflammatory mechanisms. J Biol Chem 276, 32008–32015.
Heistad DD, Wakisaka Y, Miller J, Chu Y, Pena-Silva R (2009). Novel aspects of oxidative stress in cardiovascular diseases. Circ J 73, 201–207.
Hong F, Freeman ML, Liebler DC (2005). Identification of sensor cysteines in human Keap1 modified by the cancer chemopreventive agent sulforaphane. Chem Res Toxicol 18, 1917–1926.
Huang HC, Nguyen T, Pickett CB (2002). Phosphorylation of Nrf2 at Ser-40 by protein kinase C regulates antioxidant response element-mediated transcription. J Biol Chem 277, 42769–42774.
Ishii T, Yasuda K, Akatsuka A, Hino O, Hartman PS, Ishii N (2005). A mutation in the SDHC gene of complex II increases oxidative stress, resulting in apoptosis and tumorigenesis. Cancer Res 65, 203–209.
Ito K *et al.* (2012). A PML-PPAR-delta pathway for fatty acid oxidation regulates hematopoietic stem cell maintenance. Nature Med 18, 1350–1358.
Itoh K *et al.* (1997). An Nrf2/small Maf heterodimer mediates the induction of phase II detoxifying enzyme genes through antioxidant response elements. Biochem Biophys Res Commun 236, 313–322.
Itoh K, Wakabayashi N, Katoh Y, Ishii T, Igarashi K, Engel JD, Yamamoto M (1999). Keap1 represses nuclear activation of antioxidant responsive elements by Nrf2 through binding to the amino-terminal Neh2 domain. Genes Dev 13, 76–86.
Jackson SJ, Singletary KW, Venema RC (2007). Sulforaphane suppresses angiogenesis and disrupts endothelial mitotic progression and microtubule polymerization. Vasc Pharmacol 46, 77–84.
Jeanne M *et al.* (2010). PML/RARA oxidation and arsenic binding initiate the antileukemia response of As2O3. Cancer Cell 18, 88–98.
Kang MI, Kobayashi A, Wakabayashi N, Kim SG, Yamamoto M (2004). Scaffolding of Keap1 to the actin cytoskeleton controls the function of Nrf2 as key regulator of cytoprotective phase 2 genes. Proc Natl Acad Sci USA 101, 2046–2051.
Kensler TW, Wakabayashi N, Biswal S (2007). Cell survival responses to environmental stresses via the Keap1-Nrf2-ARE pathway. Annu Rev Pharmacol Toxicol 47, 89–116.
Kim MK, Yang S, Lee KH, Um JH, Liu M, Kang H, Park SJ, Chung JH (2011). Promyelocytic leukemia inhibits adipogenesis, and loss of promyelocytic leukemia results in fat accumulation in mice. Am J Physiol Endocrinol Metab 301, E1130–1142.
Lallemand-Breitenbach V, de The H (2010). PML nuclear bodies. Cold Spring Harb Perspect Biol 2, a000661.
Lallemand-Breitenbach V, Jeanne M, Benhenda S, Nasr R, Lei M, Peres L, Zhou J, Zhu J, Raught B, de The H (2008). Arsenic degrades PML or PML-RARalpha through a SUMO-triggered RNF4/ubiquitin-mediated pathway. Nat Cell Biol 10, 547–555.
Lallemand-Breitenbach V, Zhu J, Chen Z, de The H (2012). Curing APL through PML/RARA degradation by As2O3. Trends Mol Med 18, 36–42.
Li X, Song S, Liu Y, Ko SH, Kao HY (2004). Phosphorylation of the histone deacetylase 7 modulates its stability and association with 14-3-3 proteins. J Biol Chem 279, 34201–34208.
Lin HK, Bergmann S, Pandolfi PP (2004). Cytoplasmic PML function in TGF-beta signalling. Nature 431, 205–211.
Malloy MT, McIntosh DJ, Walters TS, Flores A, Goodwin JS, Arinze IJ (2013). Trafficking of the transcription factor Nrf2 to promyelocytic leukemia-nuclear bodies: implications for degradation of NRF2 in the nucleus. J Biol Chem 288, 14569–14583.
Maul GG, Yu E, Ishov AM, Epstein AL (1995). Nuclear domain 10 (ND10) associated proteins are also present in nuclear bodies and redistribute to hundreds of nuclear sites after stress. J Cell Biochem 59, 498–513.
Melnick A, Licht JD (1999). Deconstructing a disease: RARalpha, its fusion partners, and their roles in the pathogenesis of acute promyelocytic leukemia. Blood 93, 3167–3215.
Mi L, Wang X, Govind S, Hood BL, Veenstra TD, Conrads TP, Saha DT, Goldman R, Chung FL (2007). The role of protein binding in induction of apoptosis by phenethyl isothiocyanate and sulforaphane in human non-small lung cancer cells. Cancer Res 67, 6409–6416.
Moi P, Chan K, Asunis I, Cao A, Kan YW (1994). Isolation of NF-E2-related factor 2 (Nrf2), a NF-E2-like basic leucine zipper transcriptional activator that binds to the tandem NF-E2/AP1 repeat of the beta-globin locus control region. Proc Natl Acad Sci USA 91, 9926–9930.
Moran DM, Shen H, Maki CG (2009). Puromycin-based vectors promote a ROS-dependent recruitment of PML to nuclear inclusions enriched with HSP70 and proteasomes. BMC Cell Biol 10, 32.
Mu ZM, Le XF, Vallian S, Glassman AB, Chang KS (1997). Stable overexpression of PML alters regulation of cell cycle progression in HeLa cells. Carcinogenesis 18, 2063–2069.
Myzak MC, Karplus PA, Chung FL, Dashwood RH (2004). A novel mechanism of chemoprotection by sulforaphane: inhibition of histone deacetylase. Cancer Res 64, 5767–5774.
Nishikawa T, Araki E (2007). Impact of mitochondrial ROS production in the pathogenesis of diabetes mellitus and its complications. Antiox Redox Signal 9, 343–353.
Nishikawa T *et al.* (2010). The inhibition of autophagy potentiates anti-angiogenic effects of sulforaphane by inducing apoptosis. Angiogenesis 13, 227–238.
Ohta T *et al.* (2008). Loss of Keap1 function activates Nrf2 and provides advantages for lung cancer cell growth. Cancer Res 68, 1303–1309.
Paddenberg R, Ishaq B, Goldenberg A, Faulhammer P, Rose F, Weissmann N, Braun-Dullaeus RC, Kummer W (2003). Essential role of complex II of the respiratory chain in hypoxia-induced ROS generation in the pulmonary vasculature. Am J Physiol Lung Cell Mol Physiol 284, L710–L719.
Percherancier Y, Germain-Desprez D, Galisson F, Mascle XH, Dianoux L, Estephan P, Chelbi-Alix MK, Aubry M (2009). Role of SUMO in RNF4-mediated promyelocytic leukemia protein (PML) degradation: sumoylation of PML and phospho-switch control of its SUMO binding domain dissected in living cells. J Biol Chem 284, 16595–16608.
Pham NA, Jacobberger JW, Schimmer AD, Cao P, Gronda M, Hedley DW (2004). The dietary isothiocyanate sulforaphane targets pathways of apoptosis, cell cycle arrest, and oxidative stress in human pancreatic

cancer cells and inhibits tumor growth in severe combined immunodeficient mice. Mol Cancer Ther 3, 1239–1248.
Pledgie-Tracy A, Sobolewski MD, Davidson NE (2007). Sulforaphane induces cell type-specific apoptosis in human breast cancer cell lines. Mol Cancer Ther 6, 1013–1021.
Raha S, Robinson BH (2000). Mitochondria, oxygen free radicals, disease and ageing. Trends Biochem Sci 25, 502–508.
Reineke EL, Kao HY (2009). PML: an emerging tumor suppressor and a target with therapeutic potential. Cancer Ther 7, 219–226.
Reineke EL, Lam M, Liu Q, Liu Y, Stanya KJ, Chang KS, Means AR, Kao HY (2008). Degradation of the tumor suppressor PML by Pin1 contributes to the cancer phenotype of breast cancer MDA-MB-231 cells. Mol Cell Biol 28, 997–1006.
Salazar M, Rojo AI, Velasco D, de Sagarra RM, Cuadrado A (2006). Glycogen synthase kinase-3beta inhibits the xenobiotic and antioxidant cell response by direct phosphorylation and nuclear exclusion of the transcription factor Nrf2. J Biol Chem 281, 14841–14851.
Salomoni P, Bernardi R, Bergmann S, Changou A, Tuttle S, Pandolfi PP (2005). The promyelocytic leukemia protein PML regulates c-Jun function in response to DNA damage. Blood 105, 3686–3690.
Seker H, Rubbi C, Linke SP, Bowman ED, Garfield S, Hansen L, Borden KL, Milner J, Harris CC (2003). UV-C-induced DNA damage leads to p53-dependent nuclear trafficking of PML. Oncogene 22, 1620–1628.
Sena LA, Chandel NS (2012). Physiological roles of mitochondrial reactive oxygen species. Mol Cell 48, 158–167.
Singh A *et al*. (2006). Dysfunctional KEAP1-NRF2 interaction in non-small-cell lung cancer. PLoS Med 3, e420.
Singh SV *et al*. (2005). Sulforaphane-induced cell death in human prostate cancer cells is initiated by reactive oxygen species. J Biol Chem 280, 19911–19924.
Singh AV, Xiao D, Lew KL, Dhir R, Singh SV (2004). Sulforaphane induces caspase-mediated apoptosis in cultured PC-3 human prostate cancer cells and retards growth of PC-3 xenografts in vivo. Carcinogenesis 25, 83–90.
Stuurman N, de Graaf A, Floore A, Josso A, Humbel B, de Jong L, van Driel R (1992). A monoclonal antibody recognizing nuclear matrix-associated nuclear bodies. J Cell Sci 101, 773–784.
Su YT, Gao C, Liu Y, Guo S, Wang A, Wang B, Erdjument-Bromage H, Miyagi M, Tempst P, Kao HY (2013). Monoubiquitination of filamin B regulates vascular endothelial growth factor-mediated trafficking of histone deacetylase 7. Mol Cell Biol 33, 1546–1560.
Tatham MH, Geoffroy MC, Shen L, Plechanovova A, Hattersley N, Jaffray EG, Palvimo JJ, Hay RT (2008). RNF4 is a poly-SUMO-specific E3 ubiquitin ligase required for arsenic-induced PML degradation. Nat Cell Biol 10, 538–546.
Thimmulappa RK, Mai KH, Srisuma S, Kensler TW, Yamamoto M, Biswal S (2002). Identification of Nrf2-regulated genes induced by the chemopreventive agent sulforaphane by oligonucleotide microarray. Cancer Res 62, 5196–5203.
Tong KI, Kobayashi A, Katsuoka F, Yamamoto M (2006). Two-site substrate recognition model for the Keap1-Nrf2 system: a hinge and latch mechanism. Biol Chem 387, 1311–1320.
Trachootham D, Alexandre J, Huang P (2009). Targeting cancer cells by ROS-mediated mechanisms: a radical therapeutic approach? Nat Rev Drug Discov 8, 579–591.
Venugopal R, Jaiswal AK (1996). Nrf1 and Nrf2 positively and c-Fos and Fra1 negatively regulate the human antioxidant response element-mediated expression of NAD(P)H:quinone oxidoreductase1 gene. Proc Natl Acad Sci USA 93, 14960–14965.
Wang ZG, Delva L, Gaboli M, Rivi R, Giorgio M, Cordon-Cardo C, Grosveld F, Pandolfi PP (1998). Role of PML in cell growth and the retinoic acid pathway. Science 279, 1547–1551.
Weisshaar SR, Keusekotten K, Krause A, Horst C, Springer HM, Gottsche K, Dohmen RJ, Praefcke GJ (2008). Arsenic trioxide stimulates SUMO-2/3 modification leading to RNF4-dependent proteolytic targeting of PML. FEBS Lett 582, 3174–3178.
Xu C, Yuan X, Pan Z, Shen G, Kim JH, Yu S, Khor TO, Li W, Ma J, Kong AN (2006). Mechanism of action of isothiocyanates: the induction of ARE-regulated genes is associated with activation of ERK and JNK and the phosphorylation and nuclear translocation of Nrf2. Mol Cancer Ther 5, 1918–1926.
Yamamoto T, Suzuki T, Kobayashi A, Wakabayashi J, Maher J, Motohashi H, Yamamoto M (2008). Physiological significance of reactive cysteine residues of Keap1 in determining Nrf2 activity. Mol Cell Biol 28, 2758–2770.
Zhang DD, Hannink M (2003). Distinct cysteine residues in Keap1 are required for Keap1-dependent ubiquitination of Nrf2 and for stabilization of Nrf2 by chemopreventive agents and oxidative stress. Mol Cell Biol 23, 8137–8151.
Zhang DD, Lo SC, Cross JV, Templeton DJ, Hannink M (2004). Keap1 is a redox-regulated substrate adaptor protein for a Cul3-dependent ubiquitin ligase complex. Mol Cell Biol 24, 10941–10953.
Zhang Y, Talalay P, Cho CG, Posner GH (1992). A major inducer of anticarcinogenic protective enzymes from broccoli: isolation and elucidation of structure. Proc Natl Acad Sci USA 89, 2399–2403.
Zhang XW *et al*. (2010). Arsenic trioxide controls the fate of the PML-RARalpha oncoprotein by directly binding PML. Science 328, 240–243.